Available online at www.sciencedirect.com
ScienceDirect
Journal of Power Sources 175 (2008) 686–691
JOURNAL OF POWER SOURCES
www.elsevier.com/locate/jpowsour

Short communication

Hybrid supercapacitor based on MnO_2 and columned FeOOH using Li_2SO_4 electrolyte solution

Wei-Hong Jin *, Gen-Ting Cao, Jing-Ya Sun

College of Marine Science and Technology, Zhejiang Ocean University, Zhejiang, Zhoushan 316004, China

Received 25 June 2007; received in revised form 26 August 2007; accepted 28 August 2007
Available online 16 September 2007

Abstract

The nano-sized columned β-FeOOH was prepared by the hydrolysis process and its electrochemical capacitance performance was evaluated for the first time in Li_2SO_4 solution. A hybrid supercapacitor based on MnO_2 positive electrode and FeOOH negative electrode in Li_2SO_4 electrolyte solution was designed. The electrochemical tests demonstrated that the hybrid supercapacitor has a energy density of 12 Wh kg^{-1} and a power density of 3700 W kg^{-1} based on the total weight of the electrode active materials with a voltage range 0–1.85 V. This hybrid supercapacitor also exhibits a good cycling performance and keeps 85% of initial capacity over 2000 cycles.

Keywords: FeOOH; MnO_2; Hybrid supercapacitor

1. Introduction

Nowadays, many researches on the electrochemical capacitors aim to increase power and energy density as well as lower fabrication costs while using environmental friendly materials, which can be realized by using the larger capacitance materials and/or increasing the cell voltages. The former can be realized by nano-structure or nano-size materials, which is due to that the materials with nano-size or nano-structure can provide more effective surface to produce double-layer capacitance and redox capacitance. Recently, the electrochemical capacitance of materials with nano-size or nano-structure was studied widely [1–5]. The later can be achieved with organic-based nonaqueous electrolytes that are characterized by a wider electrochemical stability window. However, despite the remarkable performance of these organic-based nonaqueous electrolytes, they suffer from the severe safety hazards. The fabrication costs of capacitors using such electrolytes are also high due to the use of a water free environment needed to manipulate and assemble. For this reason, many researches has focused on choosing proper positive electrode materials with high oxygen evolution overpotential and negative electrode materials with high hydrogen evolution overpotential to form a hybrid systems in aqueous electrolyte. Recently, several hybrid systems with aqueous solution have been developed. For example $Ni(OH)_2$/active carbon (AC) system with operation voltage range 0–1.6 V [6], MnO_2/AC system with operation voltage range 0–2.2 V [7], $LiMn_2O_4$/AC system with operation voltage range 0.8–1.8 V [8], RuO_2/AC system with operation voltage range 0–1.4 V [9] and CoAl double-layer hydroxide/AC system with operation voltage range 0.9–1.6 V [10]. For these hybrid systems, the activated carbon is typically used as one of the electrodes. However, the low density and high surface area (1000–3000 m^2 g^{-1}) of the activated carbon also limits the energy and power density of these aqueous hybrid supercapacitors. Therefore, it is most important and interesting to explore other metal oxides with a large capacitance instead of the activated carbon to form hybrid system is necessary. However, till date, the metal oxides used as negative electrode materials for these hybrid supercapacitors are rarely reported.

Recently, FeOOH has been tested as electrode materials for lithium battery. However, its electrochemical capacitance has not been studied. In present work, β-FeOOH was prepared by the hydrolysis process and its electrochemical capacitance performance was for the first time studied in mild aqueous solution. The electrochemical capacitance of hybrid supercapacitor-based

* Corresponding author. Tel.: +86 580 2550073.
E-mail address: jinwh@zjou.edu.cn (W.-H. Jin).

0378-7753/$ – see front matter © 2007 Elsevier B.V. All rights reserved.
doi:10.1016/j.jpowsour.2007.08.115

MnO_2 and β-FeOOH using mild aqueous electrolyte was also studied in detailed.

2. Experimental

2.1. Preparation of electrode materials

β-FeOOH was prepared by the hydrolysis process [11,12]. First, 10 g $FeCl_3 \cdot 6H_2O$ was dissolved in 370 ml H_2O. The 0.1 M $FeCl_3$ solution was then subjected to slow hydrolysis at the temperature 80 °C. During this process, a progressive precipitation took place. After 8 h hydrolysis, the precipitate was filtered and washed extensively with purified water. By drying at 60 °C in an oven for 12 h, the fine product was obtained. The morphology of prepared FeOOH powder was characterized by scanning electronic microscope (SEM, Philip XL30) and transmission electron microscopy (TEM, Jeol JEM-2010). For structure and phase analysis of FeOOH, X-ray diffraction (XRD) was performed using a Bruker D8 X-ray diffractometer with Cu Kα radiation (Rigaku). Electrode material MnO_2 was synthesized by directly calcining $KMnO_4$ at 250 °C for 10 h, followed by washing with distilled water.

The FeOOH negative electrode was prepared according to the following steps: the mixture containing 65 wt.% FeOOH, 30 wt.% acetylene black and 5 wt.% polytetrafluoroethylene (PTFE) was well mixed, and then was pressed onto a stainless grid (1.2×10^7 Pa) that serves as a current collector (surface is 1 cm^2). The MnO_2 positive electrode was prepared by the same method as the negative electrode described above, it consisted of 65 wt.% MnO_2, 30 wt.% carbon black and 5 wt.% PTFE. The typical mass load of positive electrode material is 5 and 10 mg of FeOOH negative electrode materials.

The electrochemical performances of the individual FeOOH electrode and MnO_2 were characterized by cyclic voltammetry (CV) and charge–discharge tests. The used electrolyte was 1 M Li_2SO_4 solution. The experiments were carried out using a three-electrode cell, in which platinum and saturated calomel electrode (SCE, 0.242 V vs. NHE) as counter and reference electrodes respectively, and it was performed using a Solartron Instrument Model 1287 electrochemical interface controlled by a computer. Hybrid capacitor test was using two-electrode glass cell, it consists of a FeOOH negative electrodes and MnO_2 positive electrode.

3. Result and discussion

3.1. The characters of FeOOH

Fig. 1 shows the XRD pattern of FeOOH prepared by the hydrolysis process. XRD intensity investigation reveals that the FeOOH was poorly crystallized. The major diffraction peaks at 2θ of 11.8°, 16.8°, 26.8°, 33.9°, 35.3°, 39.1°, 46.6°, 52.2°, 56.0°, 64.7° indicated that the prepared material has the signature of β-FeOOH which could be indexed as a tetragonal phase. β-FeOOH can be described as a tunnel-type structure comprising large channels of type 2 × 2 [12]. SEM observation (Fig. 2) showed a panorama of FeOOH, and

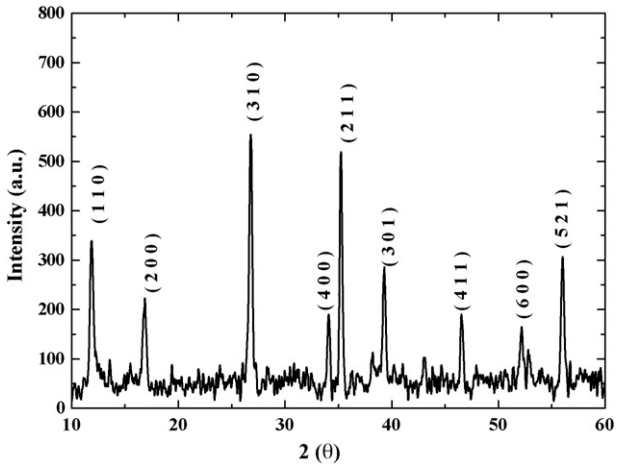

Fig. 1. X-ray diffraction pattern of FeOOH prepared by hydrolysis method.

the fine particles of FeOOH were all rod-like. It consisted of agglomerated small rods ranged from 200 to 300 nm in length, and the entire particles in view were all the same shape. To get much more detailed information, a TEM examination was taken and shown in insert. The typical size of columned FeOOH is about 40–50 nm in diameter and 200–300 nm in length.

3.2. Electrochemical characters of MnO_2 and FeOOH

The CV curves at different scan rates of FeOOH electrode within a potential window of −0.85 to −0.1 V (vs. SCE) and MnO_2 electrode within potential window of −0.1 to 1.0 V (vs. SCE) are shown in Fig. 3A and B, respectively. (The starting potential of FeOOH electrode is about −0.1 V (vs. SCE), the starting step of the CV measurement is negative sweep. The starting potential of MnO_2 electrode is about −0.1 V (vs. SCE), the starting step the CV measurement is positive sweep.). The shape of CV curves shown in Fig. 3A indicates that the capaci-

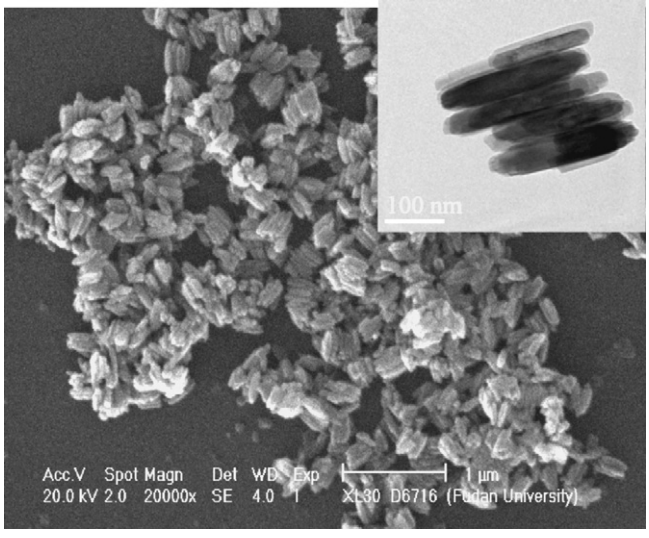

Fig. 2. SEM and TEM (insert) images of FeOOH prepared by hydrolysis method.

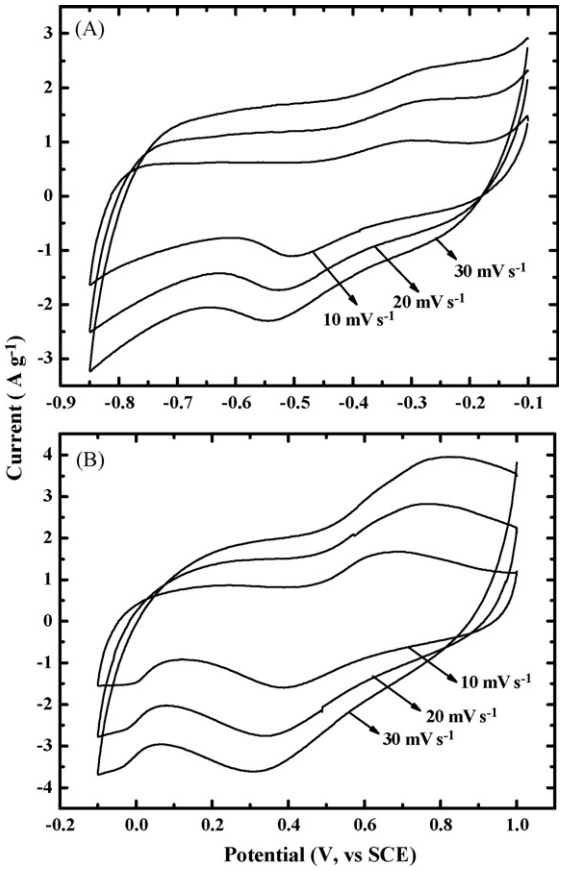

Fig. 3. CV curves of FeOOH and MnO_2 at different scan rates (10, 20 and 30mV s^{-1}). (A) FeOOH within potential window of −0.85 to −0.1 V vs. SCE and (B) MnO_2 within potential window of −0.1 to 1.0 V vs. SCE.

tance characteristic of FeOOH is distinct from that of the electric double-layer capacitance, which would produce a CV curve with close to an ideal rectangular shape. A pair of redox peaks observed in Fig. 3A indicates the redox capacitance nature of FeOOH within potential window of −0.85 to −0.1 V (vs. SCE). The reaction mechanism within FeOOH electrode can be shown as the following equation:

$$\beta\text{-FeOOH} + x\text{Li}^+ + x\text{e}^- \underset{\text{charge}}{\overset{\text{discharge}}{\rightleftharpoons}} \beta\text{-FeOOHLi}_x \quad (1)$$

Beta-iron oxy-hydroxide, which exhibits a (2×2) tunnel-type structure, can intercalate reversibly lithium in the tunnels [11]. As shown in equation (1), the discharge and charge processes occur according to the lithium intercalation and de-intercalation. It should be noted that the FeOOH electrode within aqueous electrolyte cannot realize total lithium intercalation during discharge process, which is due to the hydrogen evolution reaction within aqueous electrolyte. In organic electrolyte, FeOOH electrode can realize total intercalation reaction within potential range 3.5–1 V vs. Li^+/Li (or 0.2 V to −2.3 V vs. SCE). The result of Fig. 3B suggests the redox capacitance nature of MnO_2 within potential window −0.1 to 1.0 V (vs. SCE). The pseudocapacitive process within the MnO_2 electrode can be summarized by the following equation:

$$(MnO_2)_{\text{surface}} + A^+ + e^- \underset{\text{charge}}{\overset{\text{discharge}}{\rightleftharpoons}} (MnO_2{}^-A^+)_{\text{surface}} \quad (2)$$

where A^+ is the electrolyte cation [13]. According to the preparation process shown in the experiment section, the initial state of the prepared MnO_2 can be simplified as: $(MnO_2)_{\text{bulk}}//(MnOO^-K^+)_{\text{surface}}$. In other words, the oxidation state of the Manganese within bulk is 4^+, and the oxidation state of manganese on the surface is 3^+. The pseudocapacitance of MnO_2 electrode is based on the redox reaction occurring on the surface of MnO_2. However, as electrode materials of lithium battery in organic electrolyte, the lithium intercalation reaction in the bulk of MnO_2 mainly occurs within potential range 3.5–1.5 V vs. Li^+/Li (or 0.2 to −1.8 V vs. SCE).

The typical galvanostatic charge–discharge curves at different current density of MnO_2 electrode within potential window 0–1.0 V (vs. SCE) and FeOOH electrode within potential window −0.1 to 0.85 V (vs. SCE) are shown in Fig. 4A and B, respectively. As shown in Fig. 4A, the slope of charge curves or discharge curves of MnO_2 electrode change clearly when the redox reaction occurred. This is attributed to the potential dependent nature of faradic redox reaction. The same phenomenon

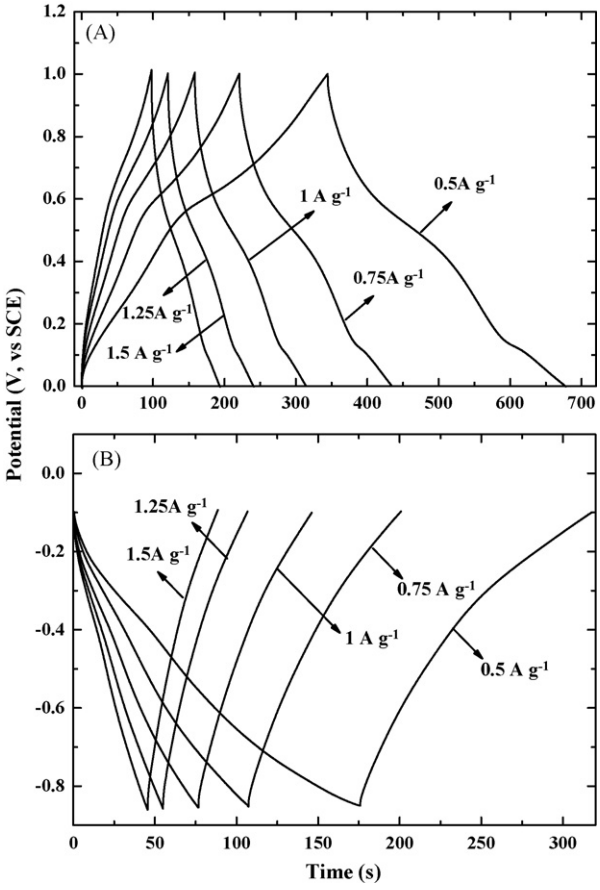

Fig. 4. Charge–discharge curves of FeOOH and MnO_2 at different current densities. (A) MnO_2 within potential window of 0–1.0 V vs. SCE and (B) FeOOH within potential window of −0.85 and −0.1 V vs. SCE.

is also observed in Fig. 4B, indicating the faradic capacitance nature of FeOOH electrode. The specific capacitances (C_m) of the FeOOH and MnO_2 at different current densities are calculated as following equation:

$$C_m = \frac{C}{m} = \frac{I \times t}{\Delta V \times m} \quad (3)$$

where I is the current of charge–discharge, t is the time of discharge. ΔV is the discharge voltage difference between the t period. The m is the mass of active materials within the electrode. The specific capacitances of FeOOH and MnO_2 as a function of different currents are compared in Fig. 5. As shown in Fig. 5, for both electrodes materials, the specific capacities decrease with the increase of charge–discharge current densities. The capacitance of the FeOOH decreases from 116 F g^{-1} (at a current density of 0.5 A g^{-1}) to 93 F g^{-1} (at a current density of 1.5 A g^{-1}), and the capacitance retention is about 80%. The capacitances of MnO_2 are 167 F g^{-1} at a current density of 0.5A g^{-1} and 143 F g^{-1} at a current density 1.5 A g^{-1}. Its capacitance retention is about 85%.

In brief, the above tests suggest that the electrochemical capacitance performance of MnO_2 is within potential window 0–1.0 V (vs. SCE) and the electrochemical capacitance performance of FeOOH is within potential window −0.85 to −0.1 V(vs. SCE). The former and the latter are characterized by high oxygen evolution overpotential and high hydrogen evolution overpotential, respectively. For this reason, it can be assumed that the hybrid system based on a positive electrode MnO_2 and a negative electrode FeOOH will increase the overall cell operating voltage. In the next section, the electrochemical capacitance of hybrid supercapacitor based on MnO_2 and FeOOH were studied in detail. For the hybrid capacitor, the weight ratio of electrode active materials (MnO_2–FeOOH) was 1:2. This ratio was calculated by considering the specific voltammetric charge and the appropriate potential windows of each material.

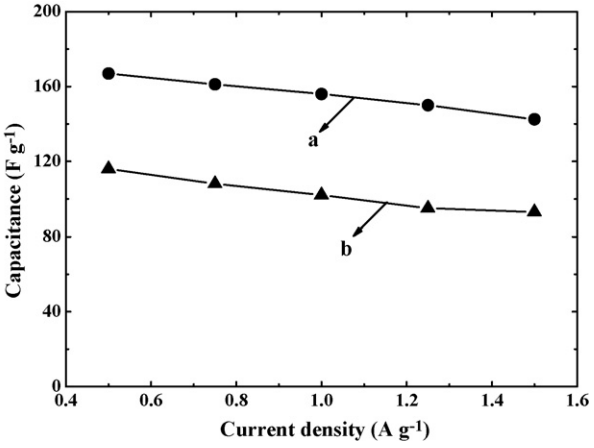

Fig. 5. Capacitance vs. charge–discharge currents: (a) MnO_2 and (b) FeOOH.

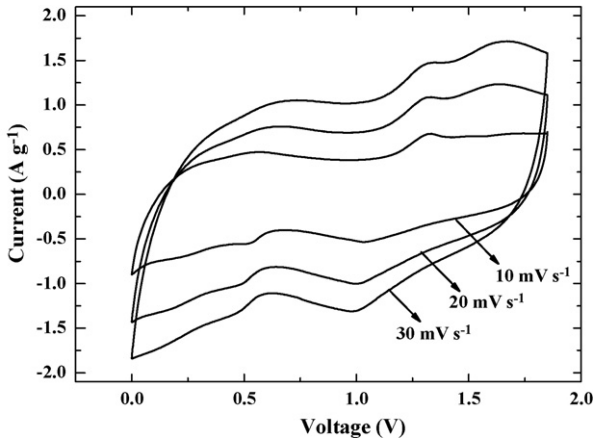

Fig. 6. CV curves of MnO_2–FeOOH hybrid supercapacitor at different scan rates within voltage range of 0–1.85 V, varying from 10, 20 to 30 mV s^{-1}.

3.3. The electrochemical capacitance performances of MnO_2–FeOOH hybrid supercapacitor

Fig. 6 shows the CV curves of hybrid supercapacitor based on MnO_2 and FeOOH at different scan rates within voltage range (0–1.85 V). As shown in Fig. 6, this hybrid supercapacitor has electrochemical capacitance behavior within the voltage range from 0 to 1.85 V. With the increase of scan rate from 10 to 30 mV s^{-1}, the shapes of CV curves of the capacitor do not change, indicating its good electrochemical performance. Furthermore, comparing the result shown in Fig. 4 and that shown in Fig. 6 suggests that choosing proper positive materials and negative materials to form hybrid systems can bring wider work voltage range. At the same time, no oxygen evolution current or hydrogen evolution current is observed in these curves shown in Fig. 6, indicating that no hydrogen evolution reaction or oxygen evolution occurs within the voltage range (0–1.85 V). Fig. 7 shows the charge–discharge curves of the hybrid supercapacitor between 0 and 1.85 V at different current densities (0.5–4 A g^{-1} of the active material). The charge–discharge curves of the hybrid supercapacitor shown in Fig. 7 are not perfectly linear as for AC capacitors, indicating its redox capacitance nature. The capacitance calculated from the discharge curves decreases from 51 F g^{-1} (at 0.5 A g^{-1}) to 26 F g^{-1} (at 4 A g^{-1}).

Fig. 8 presents Ragone plots of the MnO_2–FeOOH hybrid supercapacitor between 0 and 1.85 V. The specific power density (P) and energy density (E) of the hybrid supercapacitor were calculated as follows:

$$P = \Delta E \times \frac{I}{m} \quad (4)$$

$$E = P \times t \quad (5)$$

$$\Delta E = \frac{E_{max} + E_{min}}{2} \quad (6)$$

where E_{max} is the potential at the beginning of discharge and E_{min} the potential at the end of discharge, I the current of charge–discharge. t the time of discharge, m the mass of active materials (include positive and negative electrode) in the hybrid capacitor. The specific energy and power density

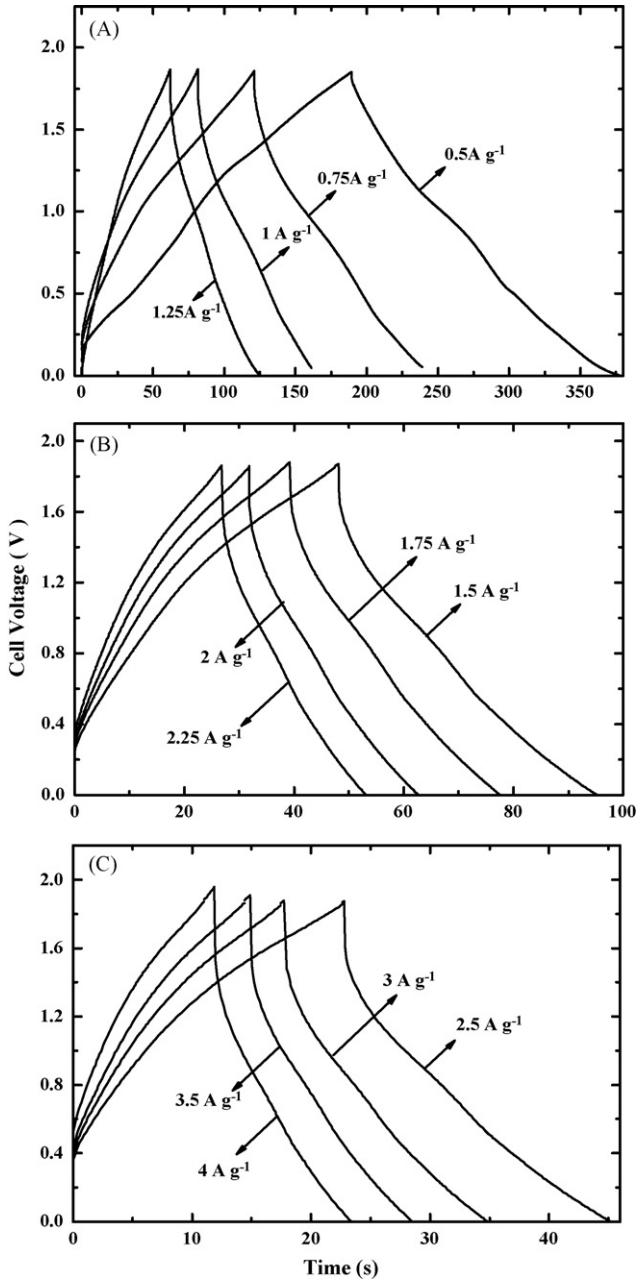

Fig. 7. Charge–discharge curves of MnO_2–FeOOH hybrid supercapacitor at different current densities within voltage range 0–1.85 V.

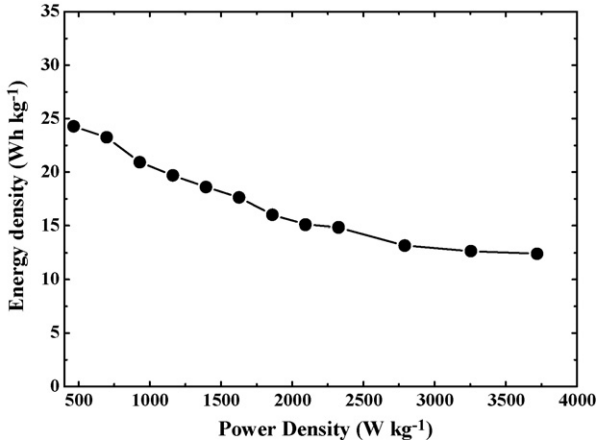

Fig. 8. Ragone plots of MnO_2–FeOOH hybrid supercapacitor.

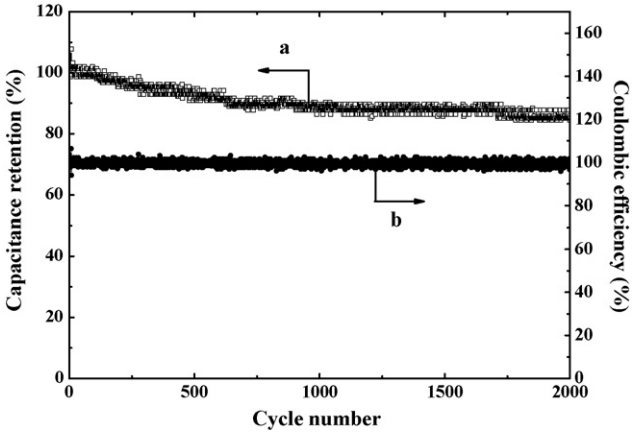

Fig. 9. Cycle life of MnO_2–FeOOH hybrid supercapacitor. (a) Capacitance retention vs. cycle number and (b) coulombic efficiency vs. cycle number.

of the hybrid capacitor shown in Fig. 8 were calculated by using the total weight of the active electrode materials. The cell voltage and the capacity based on the charge–discharge curve are shown in Fig. 7. The data of Fig. 8 clearly demonstrated that the MnO_2–FeOOH hybrid supercapacitor has a good specific energy and power density. For example, the specific energy was 24 Wh kg^{-1} at a power density of 450 W kg^{-1}, and still keeps 15 Wh kg^{-1} at a power density of 2.0 kW kg^{-1}.

Fig. 9 shows the cycling performance of MnO_2–FeOOH hybrid supercapacitor at a current of 1A g^{-1} between 0 and 1.85 V. The hybrid supercapacitor exhibits 2000 cycles with less than 15% capacity loss at an extreme cycling condition with on relaxation between cycles. The coulombic efficiency remains close to 100%, suggests that no gas evolution occurred in the cycling voltage region.

4. Conclusion

The columned β-FeOOH with 40–50 nm in diameter and 200–300 nm in length was prepared by the hydrolysis process. Electrochemical tests indicate it has electrochemical capacitance of 116 F g^{-1} within potential window −0.85 to −0.1 V vs. SCE. A hybrid supercapacitor based on positive electrode MnO_2 and negative electrode FeOOH has a wide work voltage rang (0–1.85 V) in Li_2SO_4 electrolyte solution. It delivers an energy density of 12 Wh kg^{-1} based on the total weight of the electrode active materials were obtained with at power density of 3700 W kg^{-1}. This result also indicates that choosing proper materials with high oxygen evolution overpotential and proper material with high hydrogen evolution overpotential to form hybrid supercapacitor is a promising method to increase the energy density and power density of aqueous supercapacitors.

Acknowledgments

We thank Dr. Y.G. Wang for assisting electrochemical test and Dr. Y.Y. Xia for fruitful discussions.

References

[1] Y.G. Wang, X.G. Zhang, Electrochim. Acta 49 (2004) 1957.
[2] V. Subramanian, H.W. Zhu, R. Vajtai, P.M. Ajayan, B.Q. Wei, J. Phys. Chem. B 109 (2005) 20207.
[3] V. Gupta, N. Miura, Electrochem. Solid-State Lett. 8 (2005) A630.
[4] Y.R. Ahn, C.R. Park, S.M. Jo, D.Y. Kim, Appl. Phys. Lett. 90 (2007) 122106.
[5] T. Xue, C.L. Xu, D.D. Zhao, X.H. Li, H.L. Li, J. Power Sources 164 (2007) 953.
[6] S.M. Lika, D.E. Reisner, J. Dai, R. Cepulis, Proceedings of the 11th International Seminar on Double Layer Capacitors, Florida Educational Seminars Inc., 2001.
[7] T. Brousse, M. Toupin, D. Bélanger, J. Electrochem. Soc. 151 (2004) A614.
[8] Y.G. Wang, Y.Y. Xia, Electrochem. Commun. 7 (2005) 1138.
[9] Y.G. Wang, Z.D. Wang, Y.Y. Xia, Electrochim. Acta 50 (2005) 5641.
[10] Y.G. Wang, L. Chen, Y.Y. Xia, J. Power Sources 153 (2006) 191.
[11] K. Amine, H. Yasuda, M. Yamachi, J. Power Sources 81 (1999) 221.
[12] A. Funabiki, H. Yasuda, M. Yamachi, J. Power Sources 119 (2003) 290.
[13] M. Toupin, T. Brousse, D. Belaner, Chem. Mater. 16 (2004) 3184.